

***Supporting information***

**Iron single atom catalyst anchored on nitrogen-rich MOF derived carbon nanocage to accelerate polysulfide redox conversion for lithium sulfur batteries**

Cunguo Wang,<sup>a</sup> Hewei Song,<sup>a,b</sup> Congcong Yu,<sup>b,c</sup> Zaka Ullah,<sup>d</sup> Zhixing Guan,<sup>b</sup> Rongrong Chu,<sup>a,b</sup> Yingfei Zhang,<sup>b</sup> Liyi Zhao,<sup>b</sup> Qi Li,<sup>\*,b</sup> and Liwei Liu,<sup>\*,b</sup>

<sup>a</sup> Key Laboratory of Rubber-plastics, Qingdao University of Science and Technology, Qingdao, 266042, China

<sup>b</sup> Suzhou Institute of Nano-Tech and Nano-Bionics, Chinese Academy of Sciences (CAS), Suzhou, 215123, China.

<sup>c</sup> College of Chemistry, Chemical Engineering and Materials Science, Soochow University, Suzhou, 215123, China.

<sup>d</sup> Centre of Excellence in Solid State Physics, University of the Punjab, Lahore, 54590, Pakistan.

Corresponding Email: [qli2013@sinano.ac.cn](mailto:qli2013@sinano.ac.cn) or [lqliu2007@sinano.ac.cn](mailto:lqliu2007@sinano.ac.cn).

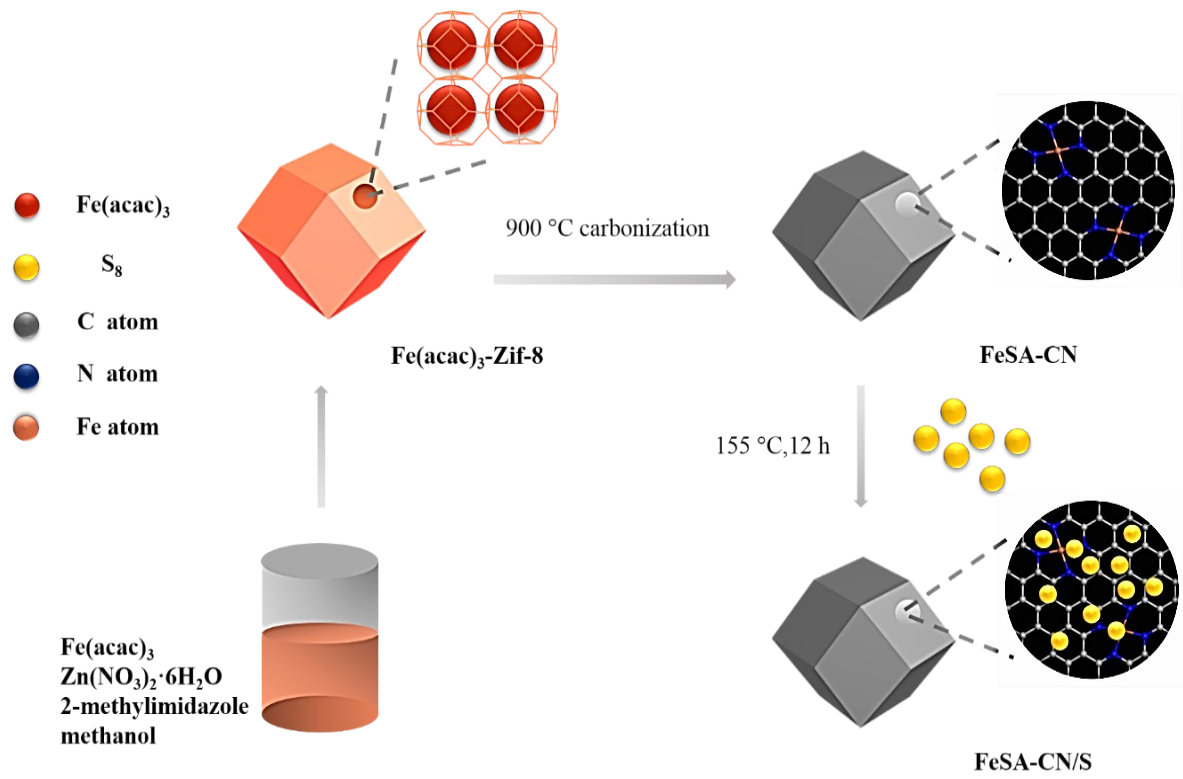


**Figure S1.** Schematic for synthesis of FeSA-CN/S.

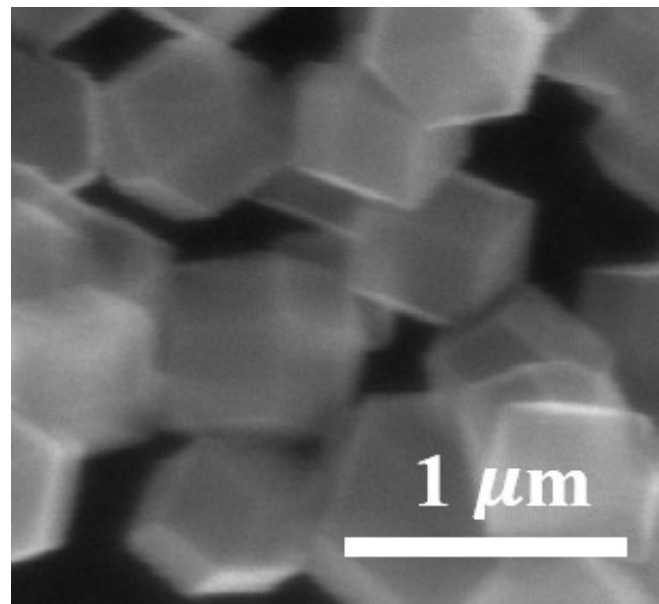


**Figure S2.** Scanning electron microscope image of CN.

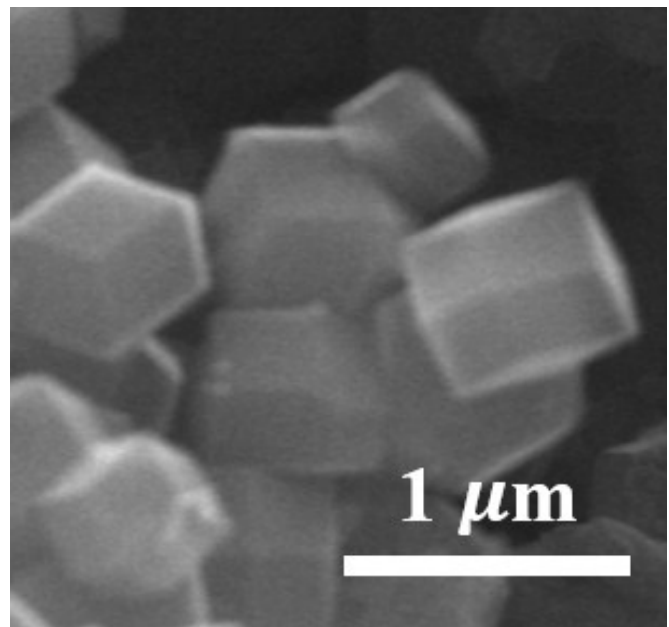


**Figure S3.** Scanning electron microscope spectrum of CN/S.

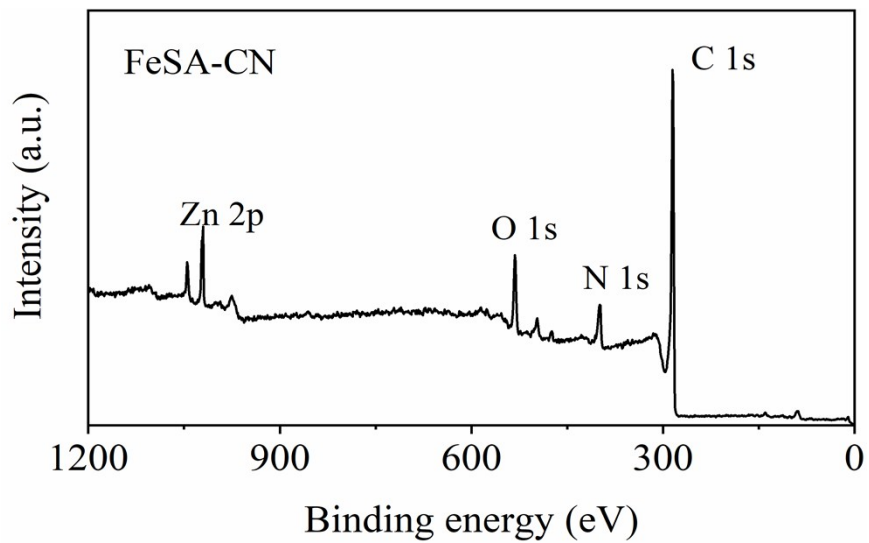


**Figure S4.** X ray photoelectron spectrum of FeSA-CN.

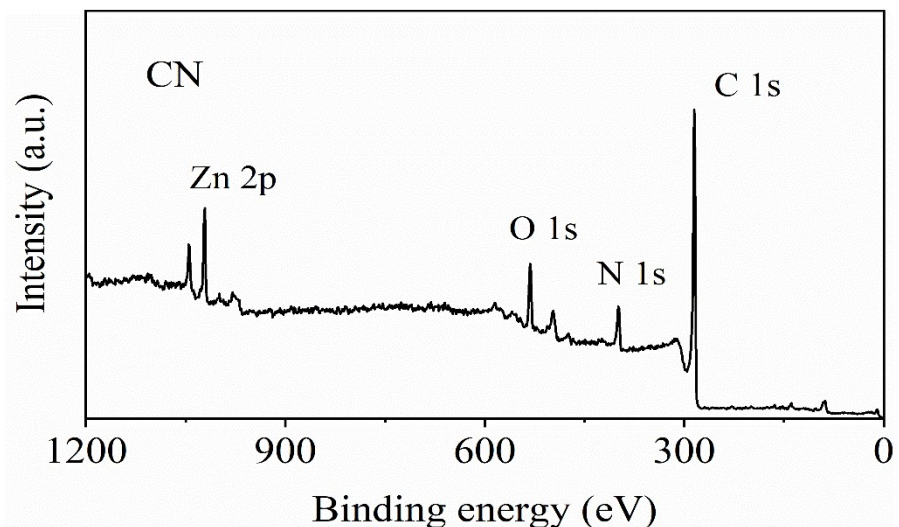


**Figure S5.** X ray photoelectron spectrum of CN.

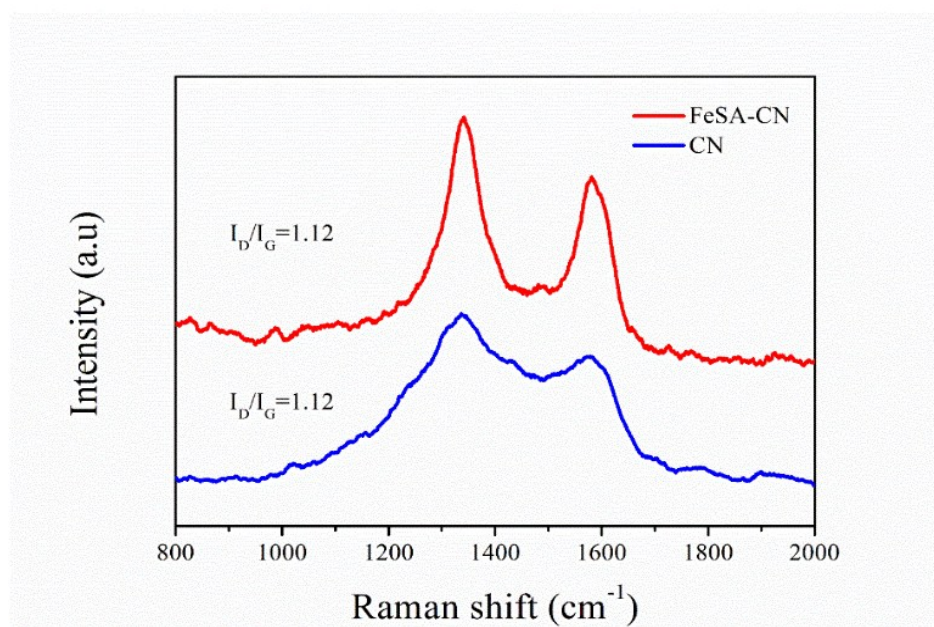


**Figure S6.** Raman spectra of FeSA-CN and CN.

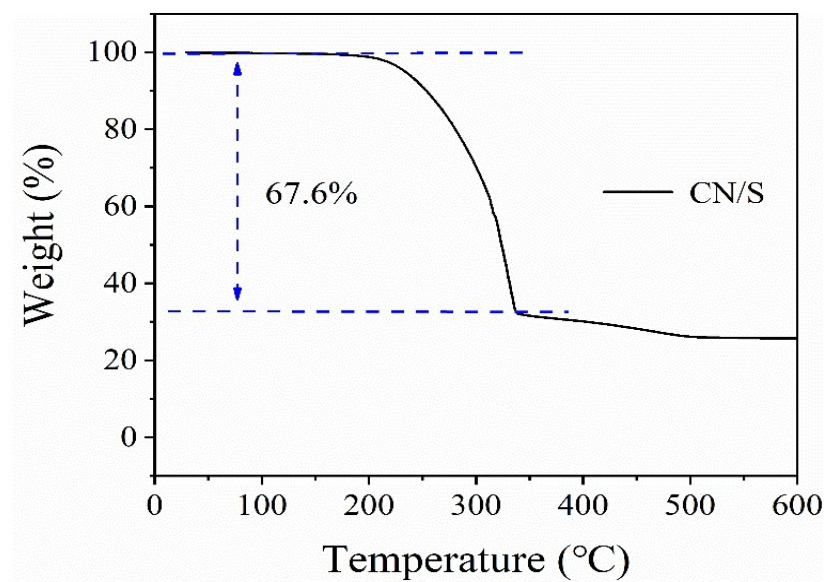


**Figure S7.** TGA curve of CN/S composite.

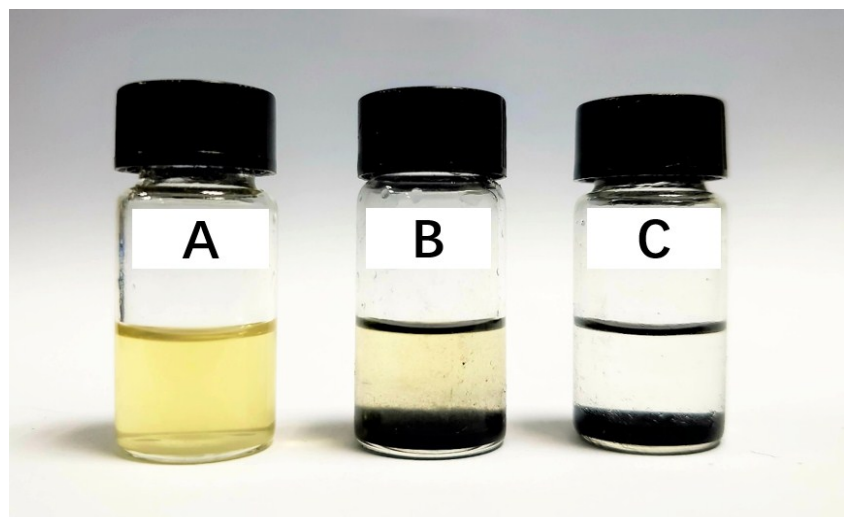


**Figure S8.** LiPSs adsorption performance measurement. Blank  $\text{Li}_2\text{S}_4$  solution (A), after the addition of CN (B) and FeSA-CN (C).

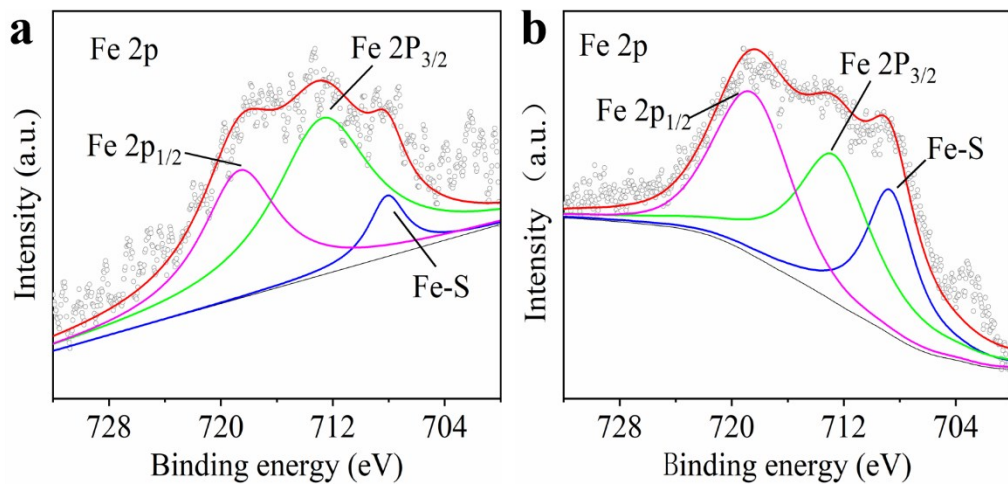


**Figure S9.** Fe 2p spectra of FeSA-CN/S electrode after fully charged (a) and during the charge process (b).

The sharp peak located at 708.5 eV is attributed to the Fe-S binding, which is closely associated with the change of Fe 2p<sub>1/2</sub> (719.5 eV). And the change of these different component Fe vividly demonstrates the periodic connection between FeSA and S<sup>x-</sup> during charge/discharge process.

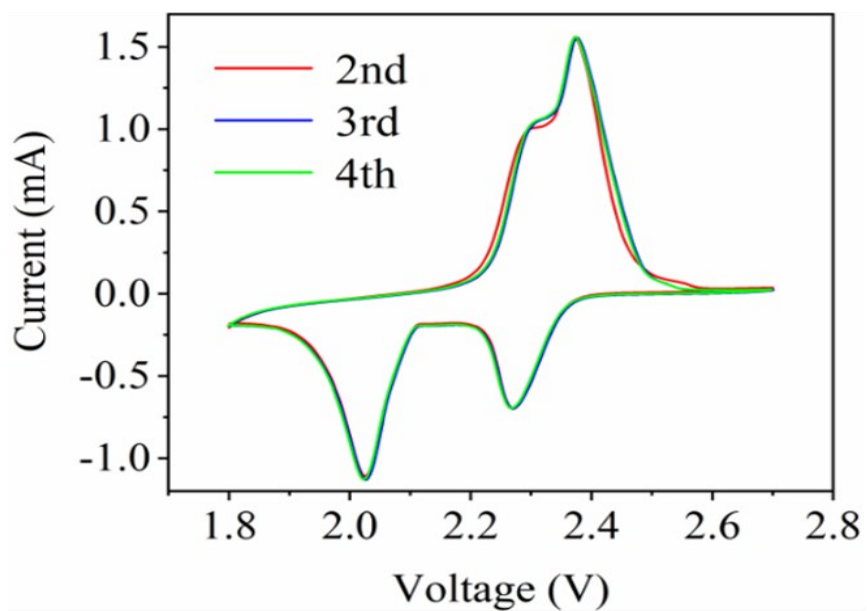


**Figure S10.** CV curves of FeSA-CN/S electrode at the scan rate of  $0.1 \text{ mV s}^{-1}$ .

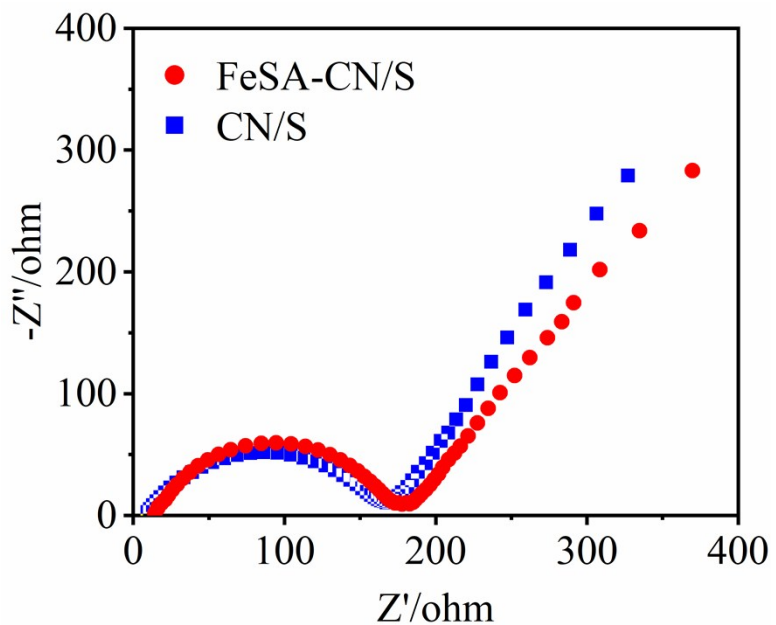


**Figure S11.** Nquist plots of FeSA-CN/S and CN/S electrodes before cycling.

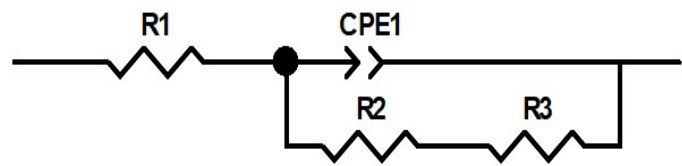


**Figure S12.** Equivalent circuit for electrochemical impedance spectra of FeSA-CN/S electrode.

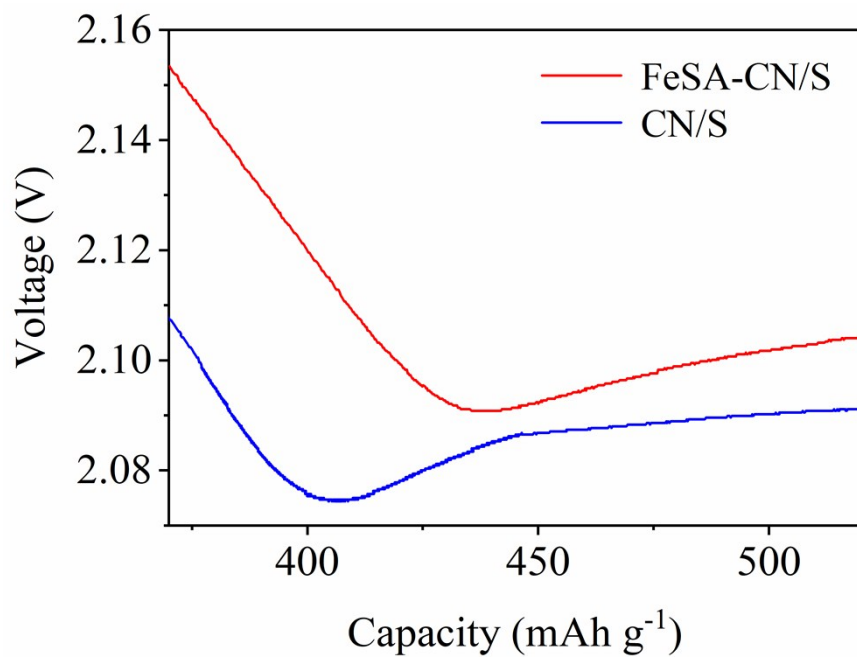


**Figure S13.** Initial period at second charge plateau of FeSA-CN/S and CN/S electrodes.

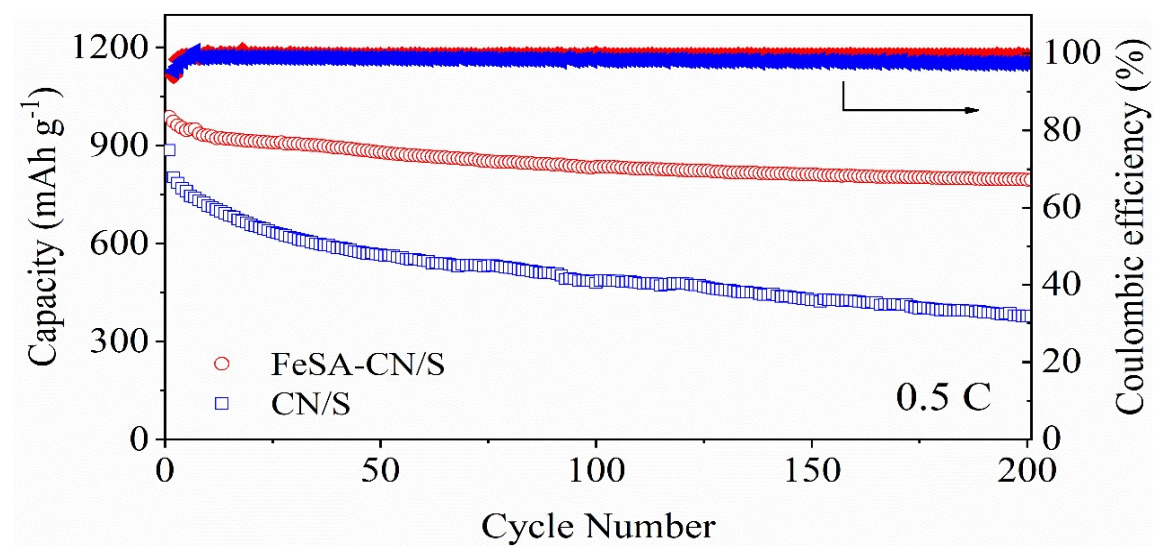


**Figure S14.** Cycling performance of FeSA-CN/S and CN/S at 0.5 C.

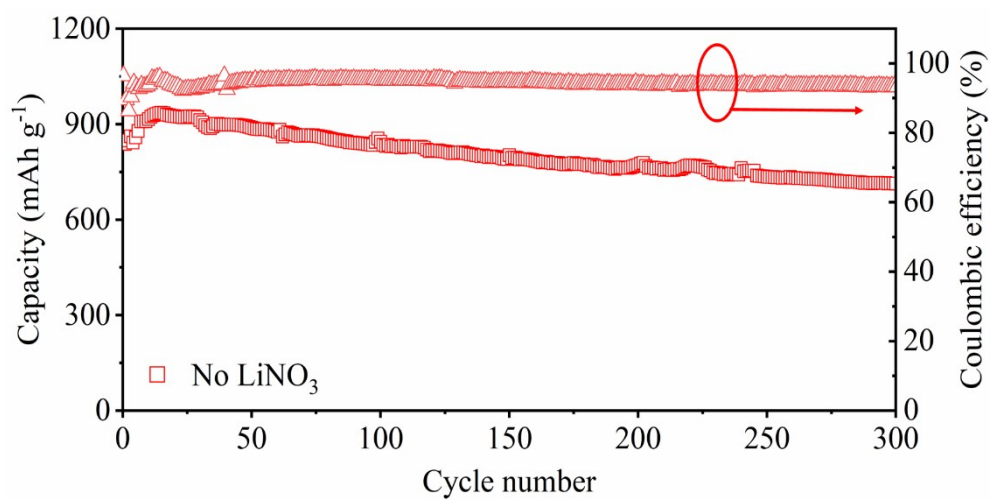


**Figure S15.** The cycling stability of FeSA-CN/S electrode at 0.5 C in the electrolyte without LiNO<sub>3</sub> additive.

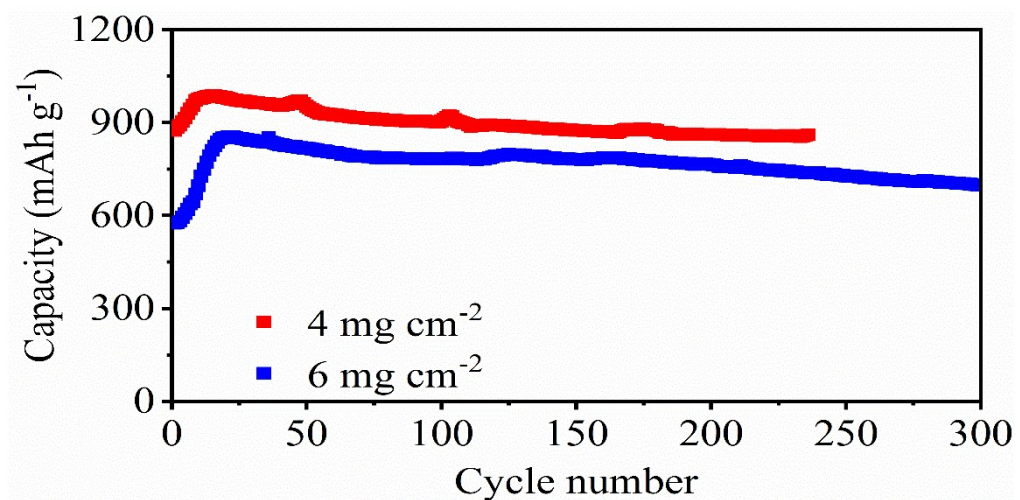


**Figure S16.** The cycling performance of FeSA-CN/S electrode with sulfur loading of 4 and  $6 \text{ mg cm}^{-2}$  at the current density of  $3.2 \text{ mA cm}^{-2}$ .

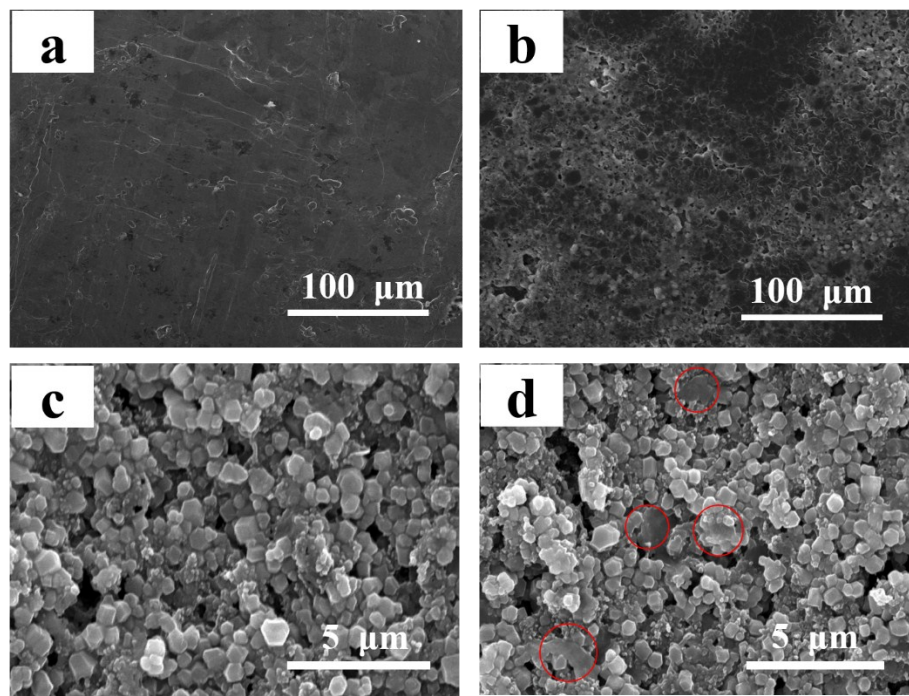


**Figure S17.** SEM images of lithium foils (a, b) and cathodes (c, d) after cycled at 0.5 C for 200 cycles. a, c) refer to the anode and cathode in FeSA-CN/S based cell; b, d) refer to those in CN/S based cell.

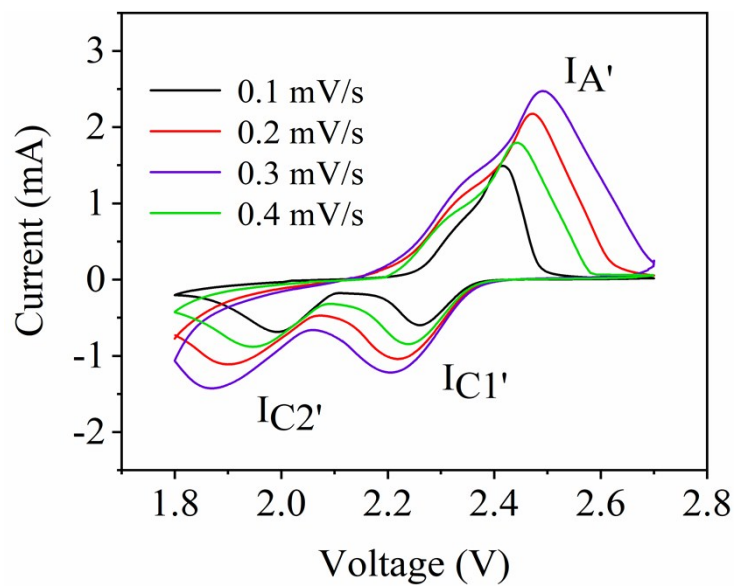


**Figure S18.** CV curves of CN/S at different scan rates.